# The Effect of Hydrogen and Hydrides on the Integrity of Zirconium Alloy Components

## Hydride Reorientation

*Author*

Manfred P. Puls
Oakville, Ontario, Canada

A.N.T. INTERNATIONAL®

© April 2018
Advanced Nuclear Technology International
Spinnerivägen 1, Mellersta Fabriken plan 4,
448 50 Tollered, Sweden

info@antinternational.com
www.antinternational.com

Ecolabelled printed matter, 441 799

## Disclaimer

The information presented in this report has been compiled and analysed by Advanced Nuclear Technology International Europe AB (ANT International®) and its subcontractors. ANT International has exercised due diligence in this work, but does not warrant the accuracy or completeness of the information. ANT International does not assume any responsibility for any consequences as a result of the use of the information for any party, except a warranty for reasonable technical skill, which is limited to the amount paid for this report.

## Quality-checked and authorized by:

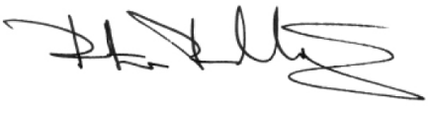

Mr Peter Rudling, President of ANT International

*Copyright © Advanced Nuclear Technology International Europe AB, ANT International, 2018.*

# Contents



*Copyright © Advanced Nuclear Technology International Europe AB, ANT International, 2018.*

*Copyright © Advanced Nuclear Technology International Europe AB, ANT International, 2018.*

# 1 Introduction

This Stand Alone Report (SAR) provides a comprehensive review and critical analysis of studies carried out to determine the conditions governing hydride orientation in tubular components made of zirconium alloys used in nuclear reactors. It is a follow-up to a recent book by the author [Puls, 2012] entitled: TheEeffects of Hydrogen and Hydrides on the Integrity of Zirconium Alloy Components: Delayed Hydride Cracking. In that book, as the title emplies, emphasis was placed on establishing the physical foundations needed to understand and predict the phenomenon of Delayed Hydride Cracking (DHC). This is a phenomenon that can occur even at low hydrogen contents in high strength zirconium alloys and is little affected by the orientations and volume fractions of hydride precipitates contained in the bulk of the material.

In the very early experimental studies of the effect of hydride precipitates on the integrity of fuel cladding and pressure tube components, the phenomenon of DHC had not yet been discovered as a possible degradation mechanism. Emphasis was placed at that time on the overall fracture toughness behaviour of the material as affected by increasing volume fraction of hydride precipitates, given that this latter phase had been found to be more brittle than the zirconium alloy matrix material in which these hydride precipitates form. It was found that the orientation of hydride precipitates plays a much more important role in determining the fracture toughness of these components than does, for instance, their volume fraction. This is because, at hydrogen contents of practical importance, hydrides form as approximately linear arrays[1] of platelet-shaped microscopic precipitates with habits on or near the basal planes of the α–Zr matrix in which they form. In the highly textured fuel cladding and pressure tube components these stringers have predominantly two tube orientations: circumferential and/or radial. In the earliest investigations of zirconium alloys used in fuel cladding and pressure tubes it was found that the fracture toughness of such tubes were significantly degraded when the orientations of the hydride precipitate clusters were in the radial direction of the tube wall compared to when their orientations were in the circumferential (hoop) direction. Hence, during the early development stages of these components, efforts were directed towards finding manufacturing processes that would result in the precipitation of mostly circumferentially oriented hydride stringers in externally unstressed tubes when cooled to temperatures at which hydride precipitation occurs. However, it was also found that a sufficiently large tensile hoop stress applied during cooling in these tubes could result in the reorientation of hydride stringers from the circumferential to the radial direction accompanied by a significant reduction in fracture toughness.

Overall, as reflected in the studies covered in this SAR, the greatest concern has been with the role of hydrides on the integrity of fuel cladding tubes rather than pressure tubes because the former components absorb considerably more hydrogen to the end of their design life during residency in the reactor than do pressure tubes, even though the residence time of the former is considerably shorter. Moreover, the continual drive by the industry to achieve greater operating efficiencies by extending the length of time between refuelling has led to the need for the development of fuel cladding components capable of maintaining their structural integrity under normal and design-basis accident conditions for ever increasing volume fractions of hydrides in the material.

In recent years emphasis has also been directed at quantifying the potential for hydride reorientation in fuel cladding tubes when these tubes are removed from wet storage and transported for placement in longer-term dry storage facilities. During dry storage of spent fuel, a hoop stress is imparted on the cladding by the inner gas pressure whilst the cladding temperature decreases gradually from several hundred degrees Celsius over several decades. Under such conditions, stress reorientation of hydride precipitates to the radial direction of the cladding tube could be possible which, then, could also make possible a severe decrease in fracture toughness of the cladding material.

As noted, the underlying physical basis of the phenomenon treated here has largely been provided in the recent book by Puls [Puls, 2012] and the reader is referred to this reference for such background. The main aim of the present account, thus, is to provide a comprehensive summary and critical

[1] Variously referred to as stringers or clusters.

Copyright © Advanced Nuclear Technology International Europe AB, ANT International, 2018.

assessment – from the earliest up to the most recent times – of the literature information on the experimental and theoretical methods used to study the factors affecting hydride reorientation.

This SAR is organized into six main sections (equivalent to chapters in a book) with the various topics in each section treated in roughly chronological order. Section 1, given here, provides a brief introduction. Section 2 summarizes the results of the earliest experimental studies on this topic. Section 3 gives an updated version of the original derivation of Ells and Puls of the theory of hydride reorientation based on classical nucleation theory. Section 4 – the longest section in this SAR, starting from the earliest to the most recent studies – deals with various applications of the Ells/Puls theoretical model to experimental data. Recent extensions to the foregoing theory are then discussed followed by accounts of other studies and methods of quantifying hydride reorientation, both in unirradiated and pre-irradiated material. A large subsection in this section is devoted to the results of *in situ* synchrotron X-ray studies. These studies have enabled real time observations of the evolution and characteristics of hydride precipitation during cooling and heating with and without external stress. Motivated by the need to interpret these results, an analysis based partially on results of Eshelby's theory of the stress state within and at the boundary of misfitting inclusions is used to explain the *in situ* observations of strain variations in hydride and matrix during heating and cooling with and without an externally applied tensile stress. Section 5 deals with theoretical computations based on the Phase Field Methodology of the evolution of hydride precipitate morphology and stress state under various thermo-mechanical cycles. These studies have been supplemented by *ab initio* atomistic models, the applications of which allow for the determination of the crystal structure and hydrogen compositions of hydride precipitates formed during the nucleation and early growth periods of hydride formation. Finally, Section 6 gives summaries of the foregoing studies, highlighting the conclusions drawn from each of these. This section is lengthier than is usually found in reports of this type, the reason for this greater length being to provide the reader with a relatively concise yet still sufficiently detailed account that it can be understood without the inclusion of all of the figures and almost all of the equations given in the preceding sections. Throughout this text, including Section 6, important findings and associated conclusions have been highlighted by placing them in italic font.

*Copyright © Advanced Nuclear Technology International Europe AB, ANT International, 2018.*

# 2 Early observations of factors determining hydride orientations

At the start of the development in the 1950s of zirconium alloy components for fuel cladding and pressure tube components there was concern that the presence of hydrides in these components could have deleterious influences on their mechanical properties. These concerns were initially allayed because studies had shown that even in material containing up to 1000 wppm hydrogen, the presence of the resultant large volume fraction of hydrides – which have up to this hydrogen content in these materials an approximately plate-shaped morphology when uniformly distributed – caused little reduction in their ductility. It was only when failures of some Zircaloy-2 fuel claddings irradiated at the Savanah River Plant, USA, showed that this failure had occurred in the heavily hydrogenated regions of the outer cladding where, locally, approximately 500 to 800 wppm hydrogen had accumulated and where hydrides had precipitated with their plate normals in the circumferential direction, did it become evident that hydride orientation with respect to the applied tensile stress axis could be an important factor in affecting the ductility of hydride-containing zirconium alloys. (Hydrides aligned with their plate normals in the circumferential direction are in the literature referred to as radial because, when viewed in optical micrographs of tube sections with normals either in the axial (longitudinal) or the radial directions of the tube show up on edge, elongated in the radial and axial tube directions, respectively. Similarly, hydrides oriented with their plate normals in the radial direction are referred to as circumferential hydrides as they have their plate edges elongated in the circumferential and axial directions.)

*Marshall and Louthan [Marshall & Louthan, 1963] showed that failure of these irradiated fuel tubes could be attributed to the radial orientation of the hydrides in the heavily hydrogenated region. The authors noted that in all previous deformation tests hydride precipitates had been oriented circumferentially such that they were approximately aligned along the externally applied tensile stress axis, with the result that these hydrides had little deleterious effects on the material's mechanical properties.*

*At about the same time as the Savannah River fuel cladding failures had occurred, a similar failure, also attributed to radially oriented hydrides, was observed in a failed swaged fuel element at the Chalk River Nuclear Laboratories, Chalk River, Canada [Parry & Evans, 1962]. To explain these results Parry and Evans analysed hydride orientations in hydrogenated (100 wppm) zirconium alloy specimens (consisting of plates, wires and sections of pressure tubes) subjected to various amounts of bending strain. The authors concluded that, comparing hydride orientation in bent and unbent specimens, hydride orientation, as exhibited by the directions of the normals to the platelet-shaped faces of the hydride clusters, is governed by the strain applied to the material, both through the retained strain produced during its manufacture and through the added amount produced by bending. They concluded that zirconium hydride platelets oriented themselves along the direction along which the material is deformed, parallel to any applied tensile strains and perpendicular to any applied compressive strains. In addition, they found that there was a limiting applied strain of about 7% below which no strain orientation of the hydrides occurred.*

In a parallel study restricted to specimens cut from Zircaloy-2 tubes Louthan and Marshall [Louthan & Marshall, 1963] showed – in agreement with the findings of Parry and Evans [Parry & Evans, 1962] – that alignment of the hydride precipitates in the as-received state depended on the type and magnitude of deformation experienced by the tubes during their manufacture. *Parry and Evans were the first to show that this alignment could be changed during hydride precipitation when the component is subjected to a suitably oriented and sufficiently large external stress. By comparing the hydride orientations found in tubes produced by different manufacturing routes before and after application of external tensile or compressive stresses these latter authors showed that manufacturing processes resulting in tube wall reduction (compression) during forming had the strongest tendency for hydrides to be aligned. The alignment in these tubes was with the plate normal of the hydrides oriented in the radial direction, i.e., the in-plane alignment of the hydride platelets was along the direction of plastic flow of the material experienced during the compression. Louthan and Marshall [Louthan & Marshall, 1963] found that there was a threshold stress that needed to be exceeded before reoriented hydrides were obtained in such materials during hydride precipitation under a tensile stress. This threshold stress was largest for tube manufacturing processes resulting in the greatest degree of*

Copyright © Advanced Nuclear Technology International Europe AB, ANT International, 2018.

*alignment of the hydride precipitates along the tube's circumferential direction when cooled under no externally applied stresses.*

The importance that hydride orientation has on the mechanical properties – shown for the first time by Marshall and Louthan [Marshall & Louthan, 1963] – resulted in a large number of subsequent studies carried out to elucidate the factors and underlying mechanisms controlling hydride orientation in tube components during normal and abnormal service conditions. The primary practical purpose of these studies was to insure that hydrides in as-manufactured pressure tubes and fuel claddings would be preferentially aligned along the circumferential-axial directions and would remain so during service under normal operating conditions.

In the first of these studies, Kearns and Woods [Kearns & Woods, 1966] subjected various (mostly) Zircaloy-4 tubing and a few plate materials to a wide range of thermo-mechanical treatments and examined the hydride orienting tendencies of these materials as a function of whether an external stress was applied or not during cooling. The objective of these studies was to better understand the role that underlying properties such as crystallographic texture, grain size, hydride nucleation sites and amount of cold work would have on hydride orientating tendencies. To determine the role of texture in affecting hydride alignment tendencies, Kearns conceived of two simpler measures that can be derived from the more detailed graphical measure of texture prevalent at the time given by the inverse pole representation. One of these measures was the volume fraction of crystals having their basal poles in a specified orientation direction with respect to a reference direction. The other measure, denoted by the parameter, "$f_d$ ", where "$d$" is a reference direction, was the determination of the resolved fraction of basal poles of the hexagonal close packed (hcp) crystallites aligned in a given reference direction. This latter measure, which has subsequently often been referred to as the Kearns factor, has found wide use as a succinct indicator of the crystallographic texture of a component in relation to its geometry. The reference directions for the foregoing measures are usually chosen as the orthogonal directions characterizing the principal directions of a sample or component. A useful property of the Kearns factors for the three orthogonal directions of a specimen or component is that their sum must equal unity. A sample having a random distribution of grain orientations is described as having no texture. In such a sample all three grain orientations would be equally represented and therefore each of the three Kearns factors would be equal to 1/3. In Zr alloys this sum rule could be useful for sample configurations such as tubes and rolled plates because$f_d$ in the working (axial or longitudinal) direction is usually less than 0.1. Hence, approximate values of the Kearns factors in the other two directions could be obtained by inverse pole figure measurements of the sample with the X-ray beam oriented in only one of the two remaining orthogonal sample directions. An example showing the relationship between the inverse pole figure characterization of texture in a plate sample with the calculated volume distribution of basal poles and their associated Kearns factors is given in Figure 2-1.

Copyright © Advanced Nuclear Technology International Europe AB, ANT International, 2018.

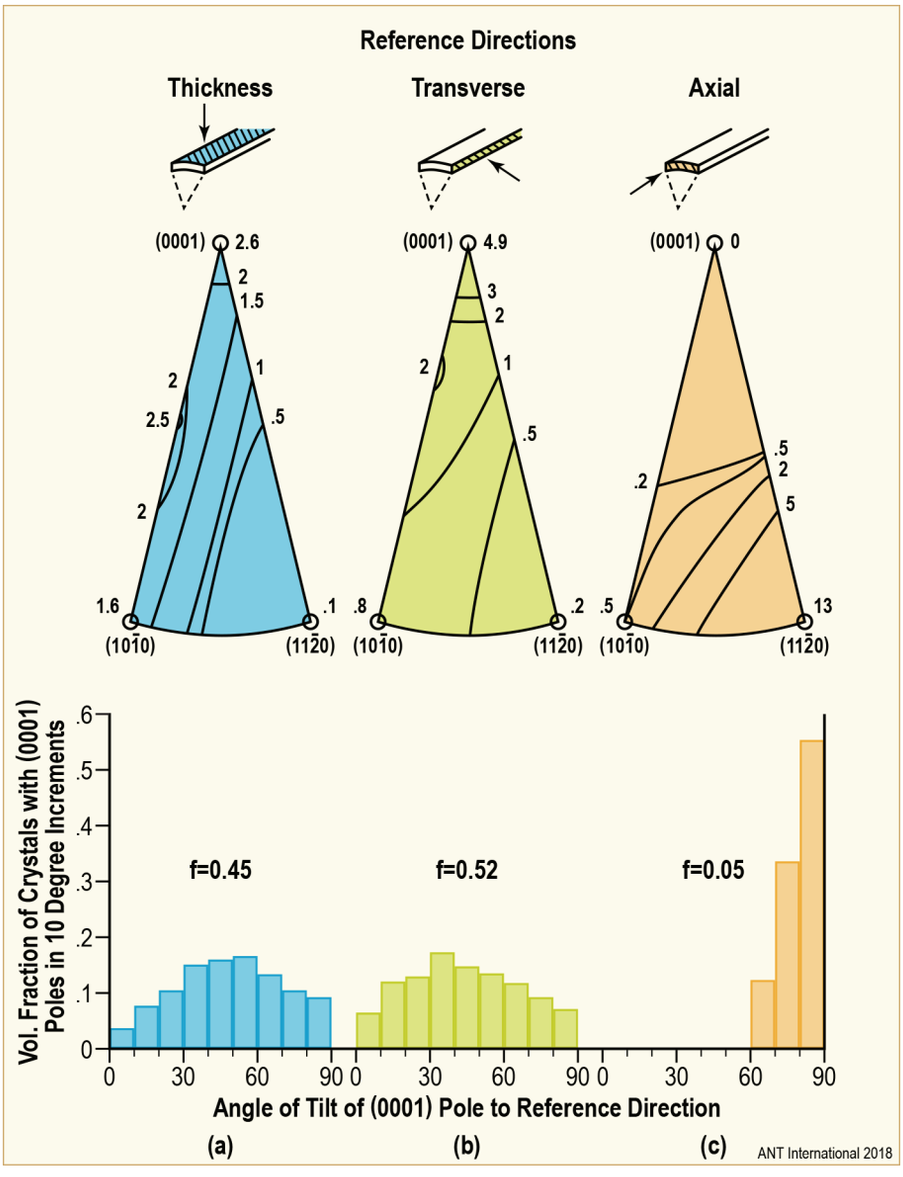


Figure 2-1: Inverse pole figure characterization of texture in tubing (from [Kearns & Woods, 1966]). Numbers on contour lines indicate orientation densities (times random) with respect to reference direction. Histograms show corresponding (calculated) volume distributions of basal poles.

Kearns and Wood [Kearns & Woods, 1966] determined that the basal pole textures in the Zircaloy materials studied depended primarily on the prior conditions of deformation rather than on subsequent annealing of the material in the alpha phase, the latter mostly altering only the orientation of poles of the $(1\ 1\ \bar{2}\ 0)_{\alpha-Zr}$ and $(1\ 0\ \bar{1}\ 0)_{\alpha-\mathrm{Zr}}$ planes. Basal poles tend to predominate in directions perpendicular to the working directions with a difference in orientation found only in the two directions transverse to the working or rolling direction. For plates, the distributions between the two directions were roughly two thirds to one third in the thickness and transverse directions, respectively, whilst the fuel cladding tubes studied by Kearns and Woods [Kearns & Woods, 1966] generally had a greater fraction of grains oriented with their basal poles in the circumferential direction. The authors point out that a key factor in the control of texture is the ratio of the diameter to wall reduction during forming. Low values of this ratio result in a larger fraction of basal poles oriented in the thickness (i.e., radial for a tube) direction whilst high values result in a larger fraction of basal poles oriented in the circumferential direction.

As was done by Louthan and Marshall [Louthan & Marshall, 1963], the authors compared the orienting tendencies of hydrides in tubes and plates when these precipitate during cooling in the

Copyright © Advanced Nuclear Technology International Europe AB, ANT International, 2018.

# 3 Theory of hydride stress orienting based on classical nucleation models

## 3.1 Overall theoretical development

The foundations of the foregoing stress orienting models of Ells [Ells, 1970] and Puls [Puls, 1984a, 1986] are derived from classical nucleation models of liquid-gas and liquid-liquid systems of Vollmer and Weber [Vollmer & Weber, 1926]. By classical is meant that – starting from the embryonic state of the new phase – there is a finite difference in structure, state and/or composition between nucleus and parent phase with a sharp interface between the two. For a system held at constant temperature below the solvus temperature, formation of the new phase is thought to occur by random statistical fluctuations of clusters (embryos) of varying sizes in which the fluctuations have produced solute compositions close to those of the equilibrium coexistence compositions between bulk quantities of the two phases. Because of the presumed sharp interface between the two phases, surface energy is created. This surface energy makes an increasing contribution to the total Gibbs free energy change for formation of the embryo as it increases in size up to a maximum value above which further increases in size result in a diminishing contribution of the surface energy change to the change in total Gibbs free energy for precipitate formation. The critical size for formation of a stable nucleus for a given undercooling below the equilibrium (bulk property) solvus is the size at which the changes in surface energy result in a maximum in Gibbs free energy change.

The earliest applications of the foregoing models to solid-solid transformations of two-component, crystalline metallic solids were mostly to substitutional solid solutions. In such systems diffusion of the two components of the solid is by a vacancy mechanism and generally involves the diffusion of both solute and solvent species at temperatures when the transformation is kinetically feasible. In substitutional solid solutions the difference in atomic radii is generally small with the result that the stress-free misfit strains (i.e., the relative differences in sizes) between the unconstrained states of daughter and parent phases are also small. In addition, with solute/solvent diffusion governed by a vacancy mechanism, at temperatures where such diffusion is rapid the misfit strains between nucleus and matrix phases is often reduced by diffusion to negligible levels by vacancy accumulation along the interphase boundary, resulting in an incoherent interface between nucleus and matrix. This is not the case expected for the Zr-H system for which one can approximate the lattice Zr atoms as being immobile with only the interstitially located H atoms in the lattice being mobile. This assumption is the basis for the classical nucleation model described in the following.

The theory for hydride stress orienting given by Puls [Puls, 1984a, 1986] follows closely the methodology developed by Sauthoff for substitutional solid solutions [Sauthoff, 1975, 1976, 1977]. The purpose of the latter author's study was to determine which of the stages of nucleation, growth and coarsening played the dominant role in stress orienting of tetragonally misfitting Au-rich, plate-shaped precipitates in the Fe-Mo-Au alloy. Unlike the initial study of stress orienting for misfitting precipitates developed by Li for the nucleation stage subsequently adopted by Ells [Ells, 1970] for the nucleation and growth stages of hydride precipitates, Sauthoff's general relationships dealt with the effect of stress on all three stages of precipitate evolution: nucleation, growth and coarsening. Moreover, Sauthoff assumed that the precipitates formed would be coherent, or partially coherent, such that they would retain at least some of their tetragonal misfit strain with the matrix. The following is a brief outline of the Ells/Puls model for hydride orientation under stress in Zr and its alloys, updated to account for the solvus relationships derived in [Puls, 2012].

In classical nucleation theory the nucleation rate is given by

Equation 3-1:

$$J^* = Z\beta^* \frac{N}{c_H^{\beta}} exp\left(-\frac{\Delta G^*}{k_B T}\right) exp\left(-\frac{\tau}{t}\right)$$

where $J^*$ = time-dependent nucleation rate (the superscript $*$ denotes quantities evaluated at the size of the critical nucleus)

$Z$ = Zeldovich non-equilibrium factor ($\approx 10^{-2}$ to $10^{-1}$)

$\beta^*$ = rate at which atoms are added onto the critical nucleus

Copyright © Advanced Nuclear Technology International Europe AB, ANT International, 2018.

$N$ = number of atomic nucleation sites per unit volume

$c_H^\beta$ = atom (or mole) solute to solvent ratio (H/Zr in our case) in the critical nucleus (where β designates the precipitate phase, which for hydrides could be either the δ, γ or ε phase)

$\Delta G^*$ = free energy of activation for critical nucleus formation

$\tau$ = incubation time

$t$ = isothermal reaction (hold) time

$k_B T$ = product of Boltzmann constant and absolute temperature, respectively

In Equation 3-1, the Zeldovich factor accounts for the fact that some supercritical nuclei decompose and that $N$ is an over estimate of the actual number of critical nuclei that can be formed at any one time.

It is assumed in Equation 3-1 that the system has been abruptly brought to a state of super-saturation determined by the magnitude of the under-cooling from the equilibrium solvus which is the solvus corresponding to bulk quantities of the two phases at the isothermal hold temperature. This means that at the start of the isothermal hold time there would exist few, if any, metastable clusters of the precipitate phase. One would then expect there to be an incubation time, $\tau$, before any critical nuclei would be formed after which there would be a short transient period of increasing nucleation rate followed by a regime during which there would be a constant (steady-state) increase in precipitate clusters. This steady state production of nuclei eventually would change to a decreasing, transient rate, terminating when the solute has been reduced to its equilibrium value.

The incubation time in Equation 3-1 is approximated by Russell [Russell, 1971] as:

Equation 3-2:

$$\tau = (2\beta^* Z^2)^{-1}$$

For hold times much greater than the incubation time, i.e., $t \gg \tau$, the bulk of the nuclei are formed at a constant, steady state rate, and it is over this regime that a meaningful comparison of the difference in nucleation rate for hydride platelets of different orientations with respect to an applied stress is obtained. That is, during steady state nucleation, the condition for the incubation time factor, $exp\left(-\frac{\tau}{t}\right) \rightarrow 1$, is assumed in Equation 3-1. With this assumption, the steady state nucleation rate, $J_{ss}^*$, is given by:

Equation 3-3:

$$J_{ss}^* = Z\beta^* \frac{N}{c_H^\beta} exp\left(-\frac{\Delta G^*}{k_B T}\right)$$

To determine the steady state nucleation rate, the factors $Z$ and $\beta^*$ need to be evaluated in addition to $\Delta G^*$.

The Zeldovich factor is given by Russell [Russell, 1968] as:

Equation 3-4:

$$Z = \left[\frac{1}{2\pi k_B T} \cdot \left(\frac{\partial^2(\Delta G^o)}{\partial n^2}\right)_{n^*}\right]^{-1/2}$$

where $n$ = number of atoms in an embryo

$n^*$ = number of atoms in the critical nucleus

$\Delta G^o$ = Gibbs free energy change for the formation of a cluster of n solute atoms

The rate, $\beta^*$, at which atoms join the critical nucleus is given by Russell [Russell, 1970] as:

Copyright © Advanced Nuclear Technology International Europe AB, ANT International, 2018.

Equation 3-5:

$$\beta^* = \frac{S^* c_H^\alpha}{d^4} D$$

where $S^*$ = disordered area of the critical nucleus (i.e., the area of the nucleus over which single solute atoms could be added)

$D$ = appropriate diffusivity

$c_H^\alpha$ = atom (or mole) solute (H) to solvent (Zr) ratio in the matrix phase

$d$ = distance of one lattice parameter

The definition of $S^*$ takes account of cases where hydride nuclei form on preferred habit plane(s) producing an ordered (coherent) interface along which single atoms arriving by diffusion cannot be added.

An explicit expression for $\beta^*$ for homogeneous nucleation of a disc-shaped nucleus at its critical dimensions was derived by Russell [Russell, 1970] as:

Equation 3-6:

$$\beta^* = 2\pi a^{*2} c_H^o N \frac{D_H^v}{d}$$

where $a^*$ = radius of the disc at its critical dimensions

$c_H^o$ = atom fraction of solute (H) in the supersaturated solution of the α–Zr phase; this is equivalent to $c_H^\alpha$ in Equation 3-5, but denoted by $c_H^o$ here to indicate that in a closed system, cooling from a temperature at which all hydrides had been dissolved, it is the total hydrogen content in the solid

$N$ = defined in the list below Equation 3-1

$D_H^v$ = volume diffusion coefficient of the solute (H)

$d$ = jump distance of solute (H) in the matrix (α–Zr) phase

The derivation of the critical nucleation energy for a material also subjected to external stress is given in Appendix A Here we summarize the results obtained. The notation used in the original publication [Puls, 1984a, 1986] has been changed in this text to be consistent with that used in this writer's recent book on DHC [Puls, 2012]. Only the treatment for plate-shaped δ–hydride precipitates is repeated here as these represent the most frequently observed final shapes and phase. For ease of calculations of the strain energy contributions to the change in Gibbs free energy upon formation of a hydride nucleus, the shape of the nucleus is approximated by an oblate spheroid of minor axis, $c$, and major axis, $a$. An oblate spheroid is not a suitable shape for accounting for the possibility that there are abrupt differences in the surface energy depending on the orientation of the surface. Thus for the purposes of accounting for the surface energy contributions to the total Gibbs free energy change, the shape of the nucleus is approximated by a disc of radius, $a$, and thickness, $2c$, and assigning different surface energy values for the faces ($\gamma_c$) and the edge ($\gamma_i$) of a nucleus having such shape. The disc is assumed to be oriented in an individual grain such that its face normal is parallel to the basal pole direction of the α–Zr matrix grain in which it is located. That is, the habit plane of the hydride nucleus is assumed to have the following crystallographic orientation relationship: $\{0\,0\,0\,2\}_{\alpha-Zr} \approx \parallel (1\,1\,1)_\delta$ and $[1\,1\,\bar{2}\,0]_{\alpha-Zr} \parallel (1\,\bar{1}\,0)_\delta$. These orientation relationships correspond to those observed experimentally for hydride precipitate sizes considerably greater than those of critical nuclei. When these orientation relationships are achieved by an invariant plane strain transformation, it is obvious that the habit plane facet is a coherent interface. It is further assumed that this facet is also coherent with the matrix when the transformation has been achieved by a pure lattice strain transformation. That is, it is assumed that the choice of transformation mode affects only the transformation strains of the hydride nucleus – and hence its strain energy – but not significantly its surface energy. In Puls' original treatment [Puls, 1984, 1986] only the latter – pure lattice strain transformation case – was specifically addressed, although the treatment is sufficiently general to include the possibility of different transformation modes and, hence, transformation strains and interphase surface energies.

Copyright © Advanced Nuclear Technology International Europe AB, ANT International, 2018.

# 4 Applications of the Ells/Puls and other theories of hydride stress orienting

## 4.1 Earliest applications of the Ells/Puls theory

### 4.1.1 Hydride stress orienting in Zr-2.5Nb material (Hardie and Shanahan, 1975)

The first application of the Ells hydride reorientation model by others to experimental data was carried out by Hardie and Shanahan [Hardie & Shanahan, 1975]. These authors carried out stress reorientation experiments in tensile specimens produced from two sources of Zr-2.5Nb material: rolled plate material and flattened pressure tube material. A problem in determining the stress orienting potency in the flattened tube material was, however, that the straightening process produced alternating macroscopic residual tensile and compressive stress zones through the thickness of the wall of the tube. In an earlier study of straightened tube specimens [Hardie & Shanahan, 1974] the authors determined that the maximum residual tensile stress occurred in a thin layer starting at the outer diameter (OD) tube wall surface and the maximum residual compressive stress occurred in a layer starting from the inner diameter (ID) tube wall surface. In specimens hydrogenated after straightening, it was found in externally unstressed specimens that the hydride distribution just at the OD surface consisted of a mixture of radial and circumferentially oriented hydrides whilst the hydride distribution at the ID surface consisted of mostly circumferential hydrides. The authors referred to these two regions as zones of mixed and stringer hydride orientations, respectively. In comparison, in hydrogenated, externally unstressed tube material that had not been straightened, the predominant hydride orientation was circumferential across the entire tube wall thickness. Measurements of the radial hydride distribution as a function of increasing applied circumferential tensile stress throughout both the mixed and the stringer zones gave a sigmoidal variation of % radial hydride fraction versus applied stress. The saturation level of % radial hydride fraction varied with the amount of total hydrogen content dissolved at the temperature at which the external stress was applied during cool down. To achieve close to 100% radial hydrides required that the temperature at which external stress was applied during cool down exceed the terminal solubility limit for hydride dissolution for the given total hydrogen content in the specimen.

To compare their results with the predictions of the Ells model the authors fitted their data for $R_x^{rad}(\sigma)$ (denoted by $R\,{}_{\boldsymbol{\sigma}}^{rad}$ by Hardie and Shanahan) to the mathematical form of the Ells equation using the relation:

Equation 4-1:

$$R_x^{rad}(\sigma) = R_o exp(B)$$

where $R_o$, $B$ = fitting constants

$\sigma$ = uniaxial tensile stress applied during the thermal cycle

With this approach $R_o$ accounts for the effect of residual stresses in the specimen through the fraction of radial hydride orientation obtained when cooled over the same temperature range under zero externally applied stress. From Equation 4-1 $F_x(\sigma, \%)$ is given by:

Equation 4-2:

$$F_x(\sigma, \%) = 100\frac{R_o exp(B\sigma)}{1 + R_o exp(B\sigma)} \equiv \frac{100}{1 + \frac{1}{R_o} exp(-B\sigma)}$$

An example of comparison between the experimentally determined dependence of $F_x(\sigma, \%)$ as a function of applied tensile stress with that predicted by Equation 4-2 is reproduced here in Figure 4-1. The figure shows that there is excellent agreement between the two, thus providing support for the validity of the physical mechanism for hydride stress re-orientation that has led to the plotted

Copyright © Advanced Nuclear Technology International Europe AB, ANT International, 2018.

mathematical form. In Figure 4-2 and Figure 4-3 similar plots of fits of Equation 4-2 to the data as those given in Figure 4-1 are shown, but without the addition of the associated data points.

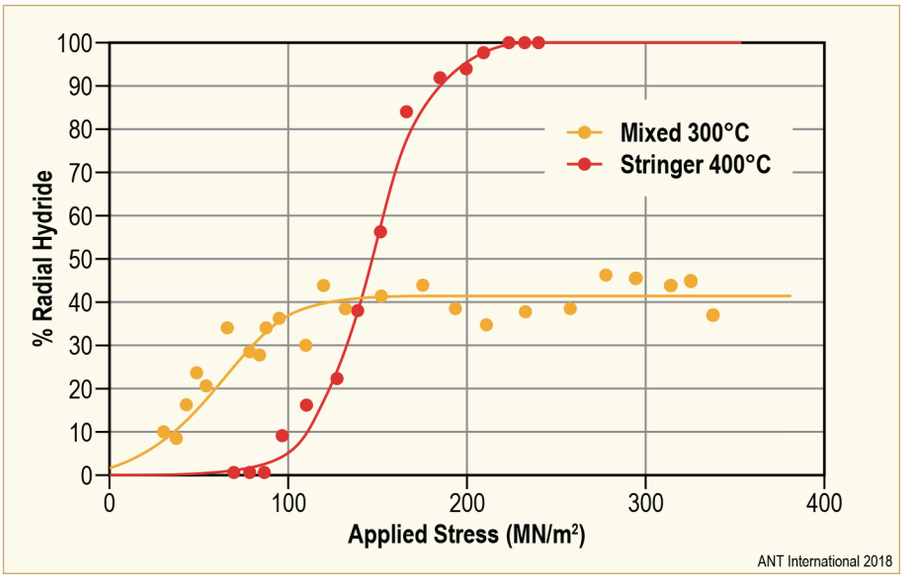


Figure 4-1: Plots of the % radial hydrides ($F_x(\sigma, \%)$) in a Zr-2.5Nb flattened tube specimen containing 100 wppm H for two different maximum temperatures from which the specimens were cooled as a function of uniaxial tensile stress applied in the tube circumferential direction (MN/m$^2$ ≡ MPa) (Series C specimen). Maximum temperatures from which the specimens were cooled are indicated in the figure (from [Hardie & Shanahan, 1975]).

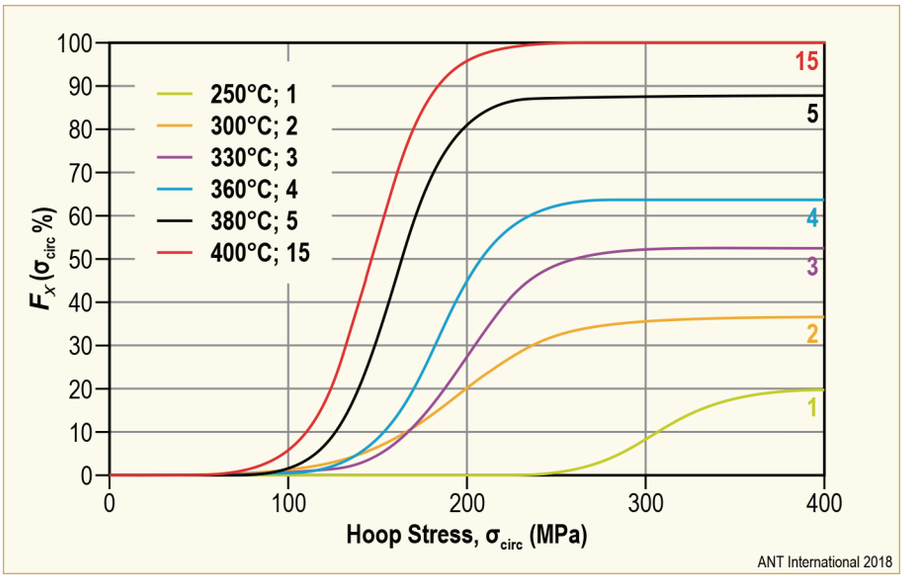


Figure 4-2: Curve fits to data of % radial hydrides ($F_x(\sigma_{circ}, \%)$) versus uniaxial externally applied tensile stress in the tube's circumferential direction for different maximum temperatures from which the specimens were cooled (from [Hardie & Shanahan, 1975]). The data used in these fits were of specimens from the ID stringer zone of flattened Zr-2.5Nb pressure tube material, all with hydrogen content of 100 wppm. The ID stringer zone is a region of maximum macroscopic residual compressive stress in the material. The number beside each curve corresponds to the specimen number in Table 2 of [Hardie & Shanahan, 1975] and to the number given in the legend showing the maximum temperature from which each of the specimens was cooled.

*Copyright © Advanced Nuclear Technology International Europe AB, ANT International, 2018.*

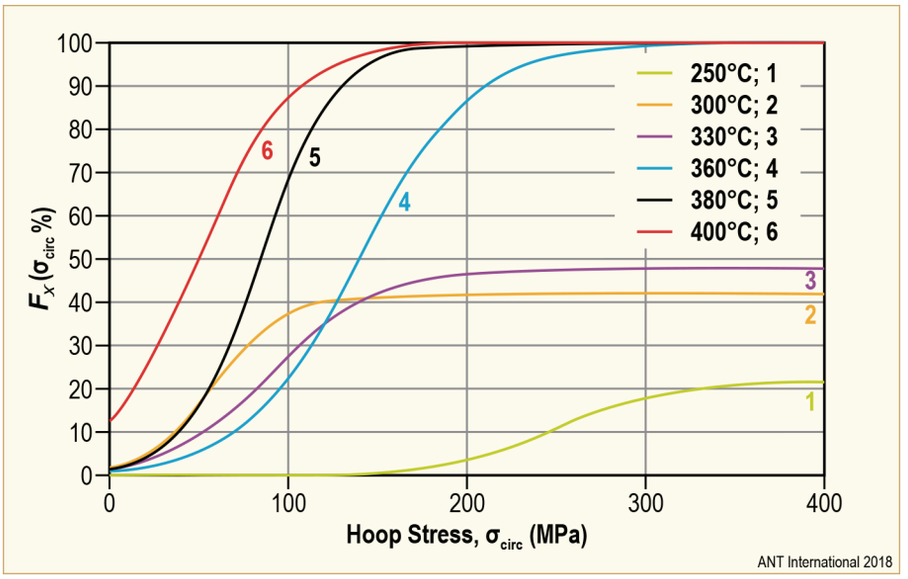


Figure 4-3: Curve fits to data of % radial hydrides ($F_x(\sigma_{circ.}\ \%)$) versus uniaxial externally applied tensile stress in the tube's circumferential direction for different maximum temperatures from which the specimens were cooled (from [Hardie & Shanahan, 1975]). The data used in these fits were of specimens from the OD mixed zone of flattened Zr-2.5Nb pressure tube material, all with hydrogen content of 100 wppm. The OD zone is a region of maximum macroscopic residual tensile stress. The number beside each curve corresponds to the specimen number in Table 1 of [Hardie & Shanahan, 1975] and to the number given in the legend showing the maximum temperature from which each of the specimens was cooled.

Note that for all of the fits given in Figure 4-2 there is an apparent lower threshold stress before there is a noticeable increase in hydride reorientation. The data for these plots were taken from the stringer zone of the flattened specimens (zone of maximum macroscopic residual compressive stress). On the other hand, for the fits plotted in Figure 4-3 – except for the data at 250°C – no lower threshold stress is indicated. The data for these plots were taken from the mixed zone of the flattened specimens (zone of largest macroscopic residual tensile stress). For the results from the stringer zone it can be seen from Figure 4-2 *that the apparent lower threshold stress (and, correspondingly, also the upper threshold stress) increases with decrease in maximum hold temperature*. For specimens with the same hydrogen content, a decrease in maximum hold temperature corresponds to a decrease in nucleation temperature. When the maximum temperature is less than TSSD, only the % of hydrogen content that is dissolved is reoriented during cooling, which accounts for the decrease of $F_x$ in the upper plateau region with decrease in maximum temperature for these specimens, all containing 100 wppm hydrogen. There is a similar trend for the results shown in Figure 4-3 for specimens from the mixed zone between the highest and the lowest maximum temperature employed, but in this case some results give the same value for the upper threshold stress (specimens 6 and 5) or a reversal (specimens 3 and 2) in the sequence with reduction in temperature. It is also evident from Figure 4-3 that the higher is the starting radial hydride fraction in a specimen the steeper is the increase in $F_x$ with increase from zero of the externally applied tensile stress.

Concentrating on two cases of specimens with hydrogen content of 100 wppm and a temperature of 400°C at which the external uniaxial stress is applied – i.e., hydrogen content and temperature of stress application exceeding the corresponding TSSD temperature – Table 4-1 gives the values of the constants obtained for these cases by Hardie and Shanahan [Hardie & Shanahan, 1975]. These values are compared with the theoretically estimated value of $B$ determined from the data of Table 3-2 and the indicated $\Delta E_{int}$ value. The theoretical plot was obtained assuming that $R_o$ in Equation 4-2 corresponds to the case of $F_x(\%)$ equal to 2% radial hydrides when the specimen is cooled under zero externally applied stress.

Copyright © Advanced Nuclear Technology International Europe AB, ANT International, 2018.

Table 4-1: Experimentally and theoretically determined parameters in Equation 4-2 for specimens containing 100 wppm H.

| Source | Stressing (Nucleation) Temperature (°C) | $10^3 R_o$ | $B$ ($10^{-6}$ Pa) |
|---|---|---|---|
| Experimental – Mixed Zone | 400 | 148 | 0.038 |
| Experimental – Stringer Zone | 400 | 0.49 | 0.037 |
| Theoretical† | (285) | 204 | 0.030 |
| †Calculated using Equation 3-42 to Equation 3-44 with $\Delta E_{int} = 0.115\sigma_{circ}$ and the data for $V_o^*$ and $T_n$ given in Table 3-2 | | | |
| © ANT International 2018 | | | |

The results summarized in Table 4-1 show reasonable agreement between the experimentally and theoretically determined exponential factors, $B$. Reasonable agreement is also obtained for the pre-exponential factors, $R_o$, between the experimental and theoretical results for which, in both cases, the starting radial hydride fraction was approximately the same ($\approx 3\%$) – as observed in the experimental example and assumed in the theoretical one. The $R_o$ factor for the experimental results from the stringer zone is considerably less compared to those of the other two cases as it incorporates the effect of the macroscopic internal residual compressive stress produced by the flattening procedure.

### 4.1.2 Hydrides in Zircaloy: Interactions between tensile stress and hydride morphology (Bai and co-workers, 1994)

The second application of the Ells model to hydride stress re-orientation data was by Bai and co-workers [Bai et al., 1994]. These authors based the analysis of their experimental results of hydride orientation in recrystallized and annealed (RXA) Zircaloy-4 sheet material on the theoretical version given by Puls [Puls, 1984a, 1986] using the simplified expression given by Equation 4-1. Tensile specimens were prepared from the Zircaloy-4 sheet material such that the tensile axis of the specimen was in the sheet's transverse direction. Figure 4-4 shows a comparison of the 'natural' and stress re-oriented orientations of hydrides in the sheet with those in a fuel cladding tube. The crystallographic texture of the specimens was similar to that in tubes, having Kearns factors of 0.65, 0.22 and 0.13 in the normal, longitudinal and transverse directions of the specimen's coordinate system. The 'natural' orientations of the plate-shaped hydrides in the tensile specimens correspond to the in-plane transverse (circumferential) orientation of the plate-shaped hydrides in the tube, whilst the stress re-oriented hydrides in the specimen correspond to radial hydrides in the tube. Hydride orientations were determined using Scanning Electron Microscopy (SEM) coupled with an image analyser. The particle orientation was defined by the angle made by the average direction of hydride segments in a cluster with the stress axis. The ratio of perpendicularly oriented hydrides (radial hydrides) was given by the percentage of hydrides having orientation angles from 0° to 30° to the total number of hydrides of all orientations. The application of the stress orienting model to their results is noteworthy in that the authors tried to account for the effect of internal grain interaction stresses produced during the forming process. Stresses and associated dislocation densities were obtained by X-ray diffraction (XRD) and Transmission Electron Microscopy (TEM). An additional feature of the stress orienting tests was that gaseous hydrogenation of the specimens at 400°C was done while a tensile stress was maintained on the (tapered) specimens. After hydrogenation to a specific H content, the specimens were cooled under stress at a rate of 1.4°C/min and the hydride orientations along the specimen length (and, hence, at different values of stress) were determined. The authors defined two tensile stress thresholds for hydride orienting: a lower threshold, $\sigma'_{th}$, which gives the applied tensile stress at which the hydride orientation first starts to change and an upper threshold, $\sigma''_{th}$, at which nearly all of the hydrides have stress reoriented. For the RXA material analysed with this hydride reorientation model, these stresses were obtained as 95 and 170 MPa, respectively. Both inter- and intra-granular hydrides were observed.

Copyright © Advanced Nuclear Technology International Europe AB, ANT International, 2018.

# 5 Theoretical evaluations of hydride precipitate morphology and stress orienting based on Phase Field Methodology

## 5.1 Introduction

In recent years, advances in numerical modelling and computing power have made it practical to use the Phase Field Methodology (PFM) as a convenient physical basis for numerical evaluations of microstructural changes. The particular advantage of the PFM is that it requires the simultaneous solution of only a few sets of equations in order to follow – and graphically map – the heterogeneous evolution with time of the microstructure from some non-equilibrium state. Tracking a particular microstructural evolution is made possible with this methodology through the introduction of "order" parameters, $\eta_p$, the numerical values of which describe the evolution of various uniquely identifiable features, $p$, of the microstructure. These parameters may or may not have a macroscopic physical meaning. Their values are chosen so that each is restricted to vary in value between zero and one. For instance, in modelling the formation of β phase precipitates from a previously homogeneous system consisting of $\alpha$ parent phase in a binary solid the order parameter is $\eta_p$ = 1 and 0 for the β and α phases, respectively, and would vary between values $0 < \eta_p < 1$ over some distance between the interfaces of these two phases. A number of order parameters, $p$, might be needed to distinguish between different variants, for instance, different orientations of the β phase in relation to the crystallographic directions of the α phase. As indicated in the foregoing, in the PFM the order parameters do not change discontinuously between matrix and precipitate. The distance over which the order parameter varies between the two phases determines the width of the interface. The phase field, then, refers to the set of values that the $\eta_p$ order parameters take throughout the chosen volume. In this method, the total free energy, $F$, of the system is described in terms of the $\eta_p$ parameters and their gradients plus equations for mass (composition), heat conduction and stress state. The order parameter is generally a non-conserved variable compared to other variables such as solute/solvent concentrations needed for the complete description of the free energy of the system. Concentrations are conserved variables and, as a result, the mathematical formulations for their temporal and spatial evolution are different compared to those for any non-conserved order parameters. A feature of this methodology is that the order parameters vary in value over some width at the α/β interfaces. As result, the PFM is often referred to as a diffuse interface model, in contradistinction to models in which the interface is taken as being atomistically sharp. Sharp interface models are thought to provide a closer representation of interfaces in real systems. However, tracking the evolution of such interfaces requires more equations compared to what is required with the PFM, particularly for complex shapes. This feature makes the solution of sharp interface models prohibitive except for highly simplified cases. PFMs could also deal with sharp interface boundaries, but the need for a corresponding sharp increase in the order parameters that would be required to describe such a sharp interface in the PFM comes at the cost of increase in computational time, which scales with the dimensions of the simulation.

It is usual in solving these types of problems with the PFM to use the time dependent Ginsburg-Landau type equation for the evolution of the non-conserved order parameters and the corresponding Cahn-Hilliard-type equation for the diffusion of the conserved solute parameter. Both of these equations, in their original form, were developed quite some ago to describe the evolution of certain types of second order (critical) phase transitions. The distinguishing feature of critical phase transitions compared to first order phase transitions is that, unlike the latter, in which there are abrupt finite changes in some of the thermodynamic variables of the system, such as the composition of the precipitating phase during the phase transformation, the onset of a critical phase transformation is characterized by the gradual, continuous disappearance or appearance of one or more thermodynamic variables – the order parameters – which become zero at the phase transition point (the critical point). In critical phase transitions, near the critical point, only small changes in the order parameter(s) (which could, for instance, also be a concentration variable) are required to change the state of the system drastically. This means that the phase transformation manifests itself through the formation of gradients of composition or order parameters, accompanied by increasing fluctuations of these composition or order parameters as the critical point is approached. To mathematically describe these effects the governing equations need to account for these gradients in order parameters and/or composition. In

Copyright © Advanced Nuclear Technology International Europe AB, ANT International, 2018.

the case of the Ginsburg-Landau equation this theory was originally developed – based on Landau's theory of second order phase transitions – to provide a phenomenological description of the transition from normal to superconductivity. In the case of the Cahn-Hilliard equation it was developed to describe spinodal decomposition of binary fluids having a miscibility gap as such systems exhibit critical behaviour at the consolute point of the phase field. Spinodal decomposition is predicted to occur in this case when the system is cooled to temperatures within the two-phase region of the phase diagram for average compositions that are inside the locus (the spinodal) defining the condition at which the second derivative of the free energy is zero. The difference between the two equations is that in the Ginsburg-Landau equation the evolution of the system is described in terms of non-conserved order parameters, whilst in the case of the Cahn-Hilliard equation it is described in terms of a conserved compositional variable. In both original applications of these equations the physical problems to which they were applied required the use of only one order parameter. However, in general, both structural and compositional variables are needed to track the evolution of a system as it evolves from its non-equilibrium to its equilibrium state. Note that when the Cahn-Hilliard equation is applied to the evolution of a first order phase transformation, the compositional gradient term takes on the role of the surface energy term as given in classical nucleation models in the latter of which the change in composition and surface boundary between the two phases is abrupt. It also means that the interface in the Cahn-Hilliard equation has a finite composition gradient, i.e., it is diffuse. The combined use of these two equations, in which both structural (non-conserved) and compositional (conserved) variables are simultaneously tracked makes it possible to graphically solve for and represent the two or three dimensional evolution of the phase transformation throughout the volume considered, with the important benefit that there is no need to specify *a priori* the morphology of the precipitates as they form or dissolve.

## 5.2 Cahn-Hilliard model of an incoherent, isotropic thermodynamic system

In the original treatment of Cahn and Hilliard for an incoherent, two-component isotropic system of volume, $V$, the Helmholtz free energy, $F$, is approximated by the sum of the Helmholtz free energy, $f'(c)$, per unit volume of a homogeneous system of composition, $c$, plus a gradient energy term defined as the difference between homogeneous and heterogeneous (actual) free energy density, $\kappa(\nabla c)^2$, *viz.* [Cahn & Hilliard, 1959]:

Equation 5-1:

$$F = \int_V [f'(c) + \kappa(\nabla c)^2 + \cdots]dV$$

with

Equation 5-2:

$$\kappa = -[\partial^2 f/\partial c \partial \nabla^2 c]' + \frac{1}{2}[\partial^2 f/(\partial|\nabla c|)^2]'$$

where the prime indicates that the spatial derivatives are to be evaluated at the limit of small $\nabla c$ and $\nabla^2 c$ so that $\kappa$ is approximately independent of the compositional gradients. Equation 5-1 and Equation 5-2 were derived by assuming that deviations from homogeneity of an initially homogeneous system can be expressed as a Taylor series expansion about the homogeneous state, $f_o$, [Cahn & Hilliard, 1958]. For a cubic lattice, or an isotropic continuum, the free energy density is invariant to the symmetry operations of reflection and rotation about a four-fold axis. This means that, to second order, the Taylor expansion of $f$ reduces to:

Equation 5-3:

$$f(c, \nabla c, \nabla^2 c, \ldots) = f_o(c) + \kappa_1 \nabla^2 c + \kappa_2 (\nabla c)^2 + \cdots$$

Hence, the total free energy is given by

Copyright © Advanced Nuclear Technology International Europe AB, ANT International, 2018.

Equation 5-4:

$$F = \int_V [f_o(c) + \kappa_1 \nabla^2 c + \kappa_2 (\nabla c)^2 + \cdots] dV$$

in which the volume integral of the gradient energy term, $\kappa_1 \nabla^2 c$, can, by the divergence theorem, be reduced to

Equation 5-5:

$$\int_V (\kappa_1 \nabla^2 c) dV = -\int_V (d\kappa_1/dc)(\nabla c)^2 dV + \int_S (\kappa_1 \nabla c \cdot n) dS$$

Since it is always possible to choose a boundary of integration such that $\nabla c \cdot n = 0$, the surface integral in Equation 5-5 vanishes, leaving only the first volume integral term. Hence the term $(\kappa_1 \nabla^2 c)$ in Equation 5-4 can be replaced with $(d\kappa_1/dc)(\nabla c)^2$ and with $\kappa = -d\kappa_1/dc + \kappa_2$, the total Helmholtz free energy reduces to the volume integral given by Equation 5-1 with $\kappa$ given by Equation 5-2.

Cahn and Hilliard point out [Cahn & Hilliard, 1959] that Equation 5-1 and Equation 5-2 should hold for any composition fluctuation capable of describing the full range of composition fluctuations resulting in the decomposition of a homogeneous phase into a two-phase mixture ranging from classical nucleation to spinodal decomposition. In the case of classical nucleation, the composition fluctuations are large in degree (amplitude) but small in (spatial) extent. Such fluctuations lead to phase separations for which there is a sharp interface (and hence large gradients) in the order parameters and composition between the two phases. As a result there is a finite (but still microscopic) energy barrier that needs to be overcome for a critical nucleus to form. Given a suitable definition of the surface energy to account for the excess gradient energy generated by the sharp interface, this is the case described by the classical nucleation model. In the spinodal decomposition case the fluctuations are small in degree but large in extent with the result that in this case there is no energy barrier other than a diffusional one for the spontaneous formation of the second phase. The compositions in the phase diagram at which this is possible are when the Gibbs free energy derivatives with respect to composition, $(\partial^2 G/\partial c^2)_{P,T} < 0$. The locus at which $(\partial^2 G/\partial c^2)_{P,T} = 0$ is referred to as the spinodal inside of which spinodal decomposition is possible. Between the spinodal and the bimodal – the latter being the locus of composition versus temperature at which the two phases are in equilibrium (i.e., the phase field locus in an incoherent mixture) – the system is metastable since finite (but still microscopic) composition fluctuations are required to overcome a finite energy barrier (the critical nucleation energy) for phase separation to occur.

Note that, unlike in the classical nucleation model where the structural characteristics and the composition of the nucleus and the surrounding parent phases are assumed to have the values of the bulk phases in equilibrium with each other (i.e., as given by the phase diagram), in the Cahn-Hilliard model of nucleation and growth, the chemical free energy, strain energy and surface (gradient) energy changes need to be determined for structural (order parameter) and composition variables having values other than those given by the equilibrium phase diagram. *Since free energy values away from the equilibrium state of the system are rarely known, this is one of the weaknesses of this model for quantitative application when applied to phase transformations under conditions conforming more closely to the classical nucleation model of phase separation.*

## 5.3 Application of PFM to hydride precipitates in zirconium

Shi and co-workers were the first to apply the PFM to simulate the morphological development and orientation of hydride precipitates in externally stressed and unstressed zirconium material. The earliest such paper is that of Ma and co-workers [Ma et al., 2002]. In this paper the shape and orientation of γ–hydride precipitates forming during their nucleation and growth stages with or without externally applied stress is evaluated. This study was restricted to the formation of the γ–hydride phase because the symmetry in the transformation strains of this phase with respect to the α–Zr matrix [Carpenter, 1973] allows the problem to be solved in two dimensions. γ–hydride

Copyright © Advanced Nuclear Technology International Europe AB, ANT International, 2018.

# 6 Summary and Conclusions

The summary and conclusions given here are longer than one would normally expect to find in a report of this type. It was felt, however, that the information provided up to this point – covering the totality of the field from its inception to its present time – is so varied and complex that a concise but yet sufficiently detailed summary was in order. The aim was to provide a reasonably self-contained account that, nevertheless, provided sufficient detail for its content to be readily understood without reference to any of the figures, tables and almost all equations given in the preceding sections. Because this section is still quite lengthy, it has been subdivided into subsections that correspond to similar ones given in the preceding sections.

## 6.1 Early Work

From early studies carried out at the start of nuclear reactor development in the 1950s to the end of the 1960s, a number of key observations concerning hydride orientations in tubes had already been established. These observations are:

a) Hydrides formed under slow cooling conditions show up as irregularly shaped elongated stringers when viewed at optical magnifications. (A hydride stringer is defined here as a collection of closely clustered smaller platelet-shaped hydride precipitates, the thickness, length and distribution of which depend on the material's texture, hydrogen content and cooling rate.)

b) *In externally unstressed tubes manufactured for reactor application, hydride stringers are preferentially oriented with their traces in the circumferential/axial tube directions.* The shapes and orientations of the broad outlines of these stringers are similar to those of the grains in which they are contained. Selected observations indicate that these transverse stringers consist of a collection of clusters of short individual hydrides, frequently tilted ≈ 45° to the circumferential tube direction in the circumferential-radial plane.

*c) Uniaxial tensile stress applied during cooling over temperature ranges where hydride precipitation occurs produces hydride stringers oriented with their traces perpendicular to this stress and parallel to the direction of compressive stress.*

*d) Stress applied during isothermal hold* after a cool down (during which there would be no further hydride precipitation) *does not affect the existing distribution of hydride orientations.*

e) Reorientation of hydride stringers from circumferential to radial direction by an external tensile stress applied in the circumferential direction during hydride precipitation requires that the applied stress exceed a threshold stress. Above this threshold stress value, the proportion of reoriented hydride stringers measurably increases with increase in the magnitude of the external tensile stress.

f) The smaller hydride platelets making up a stringer were found to reside on similar, preferred habit planes with respect to the α–Zr matrix grains in which they were located. The individual hydride habit planes are the same irrespective of whether the macroscopic orientations of the stringers were changed with application of an external stress.

g) In commercial α– and α/β–zirconium alloys (Zircaloy and Zr-2.5Nb, respectively) the habit planes of hydride platelets – as deduced from optical observations of hydride stringers – are oriented 5 to 20° from the basal pole direction of the α–Zr matrix grains in which they form. This result is consistent with hydride habit planes of $\{1\ 0\ \bar{1}\ 7\}_{\alpha-Zr}$ (≈ 14° from the basal pole direction) determined subsequently in these alloys.

*h) Based on the information given in items a) to f), it was concluded that the observed preferred circumferential orientation of hydride stringers in externally unstressed, cold-worked, fine-grained material occurs because of the presence of internal tensile stress generated in the radial tube wall direction in grains oriented with their basal pole oriented in the radial direction or compressive stress in the circumferential direction of grains with their basal poles oriented in the circumferential direction. It is conjectured that these internal tensile or compressive stresses are produced during the reduction in wall thickness of the tubes during the cold*

Copyright © Advanced Nuclear Technology International Europe AB, ANT International, 2018.

*working step under conditions resulting in only a small reduction in tube diameter. In this case, plastic flow in the tube would be directed in the circumferential direction.*

i) The fraction of hydrides that can preferentially orient under a tensile stress in a given direction is limited by the availability of grains having favourable basal pole orientations. In general, the basal pole fraction in any direction that would be limiting for complete preferential hydride orientation would depend – in addition to the grain size – on the total volume fraction of hydrides at the precipitation temperature. In tubes in which the Kearns factor is generally less than 0.1 there are insufficient grains with basal pole orientations in the axial direction for stress-reorientation of hydrides with their platelet normals pointing in this direction.

## 6.2 Theoretical Model

For the determination of hydride nucleation rate under zero stress an expression was developed based on classical nucleation theory. The classical model involves developing an expression for the increase in Gibbs free energy of formation of a hydride nucleus of critical dimensions. To account for the effect of stress on the resultant change in critical nucleation energy, an approximate solution (see Equation 3-18 to Equation 3-28) was derived that applies when the change in net interaction energies for hydride formation of a nucleus of critical size is much less than the sum of the changes in chemical and strain energies for this formation. In this case, the total Gibbs free energy change for hydride nucleus formation is simply the sum of the Gibbs free energy change for nucleus formation under zero stress plus the Gibbs free energy change for formation under stress. In the classical model, the nucleation rate is proportional to an exponential term with exponent given by the total Gibbs free energy change of formation of a nucleus of critical size divided by the usual product of Boltzmann constant and absolute temperature at the nucleus formation temperature. Hence, in this approximation the nucleation rate is proportional to the product of the usual hydride nucleation rate expression under zero stress multiplied by an additional exponential term with exponent given by the product of the volume of the critical nucleus under zero stress times the net interaction energy change for formation of this nucleus. In a closed thermodynamic system the net interaction energy change is given by the interaction energy change for hydride formation minus the interaction energy change under the same stress for removal of hydrogen in solution to form this hydride. The latter interaction energy change was modified from the original solution by Puls to account for the anisotropy of the transformation strains of hydrogen in solution. This anisotropy arises from the crystallographic anisotropy of the interstitial sites of the hcp α–Zr lattice in which the hydrogen atoms reside.

The approximate solution of the Ells/Puls model for hydride nucleation under non-hydrostatic stress predicts that an increase in the volume of the critical nucleus increases the potency of the effect of stress on hydride reorientation, but with an associated decrease in nucleation rate. A corollary to this is that when the rate of increase in hydrogen supersaturation is slow, such as at very slow cooling rates or for hydrogen diffusion to local regions of elevated stress or decreased temperature, the potency for hydride reorientation is increased. The magnitude of the critical nucleation volume depends on the hydride's surface energy, the increase in chemical driving energy with decrease in temperature below the incoherent solvus (or, conversely, with increase in hydrogen concentration above the incoherent solvus) and the strain energy of the nucleus. The latter depends on the shape of the critical nucleus and its transformation strains with these transformation strains depending, in turn, on temperature and hydrogen composition of the critical nucleus with the hydrogen composition of the latter also depending on temperature.

The model predicts that during precipitation hydride reorientation under a uniaxial tensile stress would occur when the net interaction energy change for the reoriented hydrides is less than that for hydride orientation under zero external stress.

If the difference in interaction energy change for hydride formation and hydrogen removal under the same stress is positive then application of an external tensile stress enhances the nucleation rate compared to the nucleation rate at zero external stress. However, this is the case only if there is a difference in partial molar volumes or transformation strains between hydrogen in solution and in hydride precipitates. The earliest models developed to account for the effect of stress on hydride orientation as given by Ells, and for other materials by Sauthoff, neglected to include the change in interaction energy of hydrogen atoms removed from solution to form hydrides or, in the model by Sauthoff, Au solute atoms removed from solution to form Au-rich precipitates. The subsequent

Copyright © Advanced Nuclear Technology International Europe AB, ANT International, 2018.

treatment by Puls included this term but assumed that the transformation strains of the removed hydrogen atoms in solution are isotropic. In this case, the theory predicts that there would be no difference in the strength of the stress orienting effect, whether or not the contribution to the net interaction energy of the removal of hydrogen in solution is included. This is because, if hydrogen atoms in solution have isotropic transformation strains, there is no difference in interaction energy for the removal of these atoms regardless of the orientation of the external stress with respect to the orientation of the hydrides. Therefore the predictions for the interaction energy difference between unreoriented and reoriented hydrides are the same in both the original Ells and subsequent original Puls hydride nucleation models.

In estimates of the potency of stress reorientation the inclusion of the anisotropy of the transformation strain matrix of hydrogen in solution means that the contribution to the interaction energy arising from the removal of hydrogen atoms in solution affects the difference in interaction energies between circumferentially and radially oriented hydrides. However, inclusion of this interaction energy term also creates an uncertainty in the predictions of the model for the magnitude of the stress reorienting effect since it results in the prediction that there could be two possible bounding solutions. One bounding solution is based on the assumption that hydrogen removed from solution for hydride formation in a given grain comes from either the same grain or from near-by grains having identical orientations with respect to the direction of the externally applied stress (i.e., they are part of the same (closed) thermodynamic system). Alternatively, a larger interaction energy difference for hydride reorientation is achieved if the hydrogen atoms required for forming the hydride nuclei are assumed to come predominantly from grains in which the chemical potential of hydrogen in solution (diffusible hydrogen) is greater than it is in the grains in which the reoriented hydrides are formed.

In summary, preferential, stress assisted hydride reorientation during nucleation occurs because the transformation strains of hydrogen in solution and hydride precipitates are anisotropic with the governing anisotropy being that of the transformation strains of the hydride precipitates. Hydrides aligned with their plate normals in the direction of a uniaxial tensile stress are predicted to have lower negative interaction energy and, hence, greater nucleation rate, than those aligned in the other two orthogonal directions.

For the simplest case of a material having a crystallographic texture consisting of only two sets of grain orientations, one set of grains having basal poles oriented in the radial direction, the other set of grains having basal poles oriented in the circumferential direction, the present model for stress assisted hydride reorientation shows that when the source of hydrogen in solution to form hydrides comes from the same set of grains in which the hydride precipitates are formed, the difference in interaction energies for hydride formation in the two sets of grains is much reduced compared to the case if the transformation strains of the hydrogen atoms in solution had isotropic symmetry. In this latter case only the transformation strains for hydride formation enter into the difference in interaction energy between the two orientations. A similar result as the latter is, however, also obtained when taking account of the anisotropy of the transformation strains of hydrogen atoms in solution when these atoms come from grains that have their basal poles at right angles to the grains in which preferential, stress-driven hydride precipitation occurs.

It is evident from the foregoing that there can be large quantitative differences in the predictions for the orienting potency of hydride precipitates under stress depending on the differences in magnitudes of the three dilatational components of transformation strains for hydride formation. Two sets of transformation strain matrices are in current use in the literature. The set with the least amount of anisotropy is derived assuming hydride formation occurs via a pure lattice strain transformation. The other set with the greatest amount of anisotropy was derived assuming that hydride formation occurs via an invariant plane strain transformation. In this case all of the volumetric strain for hydride formation is directed in the direction of the hydride precipitate's plate normal with the other two transformation strains in the plane of the plate approximately equal to zero. No direct experimental evidence exists to verify which of these two proposed sets of transformation strains occurs in reality. Further on, results of atomistic models of hydride formation are discussed that attempt to shed light on this uncertainty.

Both sets of transformation strain matrices predict that under a uniaxial tensile stress directed in the circumferential direction of a tubular component there would be an increase in temperature at which radial hydrides (hydrides with their normals in the circumferential direction) first precipitate compared

Copyright © Advanced Nuclear Technology International Europe AB, ANT International, 2018.

# References

Alam A.M. and Hellwig C., *Cladding Tube Deformation Test for Stress Reorientation of Hydrides,* J. ASTM Int. 5, Paper ID JAI101110, 2008

Aomi M. et al., *Evaluation of Hydride Reorientation Behaviour and Mechanical Properties for High-Burnup Fuel- Cladding Tubes in Interim Dry Storage*, Journal of ASTM International, Vol. 5, Issue 9, Paper ID JAI101262, 2009.

Babayak W.J., *Hydride Habit in Zirconium and in Unstressed and Stressed Zircaloy-4,* Trans. Met. Soc. AIME 239, p. 252, 1967

Bai J. Gilbon J., Prioul C., Francois D., *Hydride Embrittlement in Zircaloy-4 Plate: Part II. Interaction Between the Tensile Stress and the Hydride Morphology*, Met. and Materials Transactions, Vol. 25A, p. 1199, 1994.

Bailey J.E., *Electron Microscope Observations on the Precipitation of Zirconium Hydride in Zirconium,* Acta Metall. 11, p. 267, 1963

Beck R. L., *Zirconium-Hydrogen Phase System*, Trans. ASM 55, 542–555, 1962.

Billone M., Bursteva T.A. and Liu L., Argonne National Laboratory Report, ANL-12-58, 2012

Blat-Yrieix M. et al., *Toward a Better Understanding of Dimensional Changes in Zircaloy-4: What is the Impact Induced by Hydrides and Oxide Layer?*, 15th Zirconium in the Nuclear Industry, ASTM, Sunriver, OR, June 2007 and Journal of ASTM International, Vol. 5, No. 9 Paper ID JAI101321, www.astm.org

Borisov V.T., Golikov V.M. and Scherberdinsky G.V., Phys. Met. Metall. 17, p. 80, 1964

Bouffioux P., *Réorientation des Hydrures – Synthèse des Résultats Acquis pour les Gaines en Zircaloy-4* AFA-2G, EDF Report HT25-C2002-191/PB, 2002

Cahn J.W. and Hilliard J.E., *Free Energy of a Nonuniform System. I. Interfacial Free Energy*, J. Chem. Phys. 28, p. 258, 1958

Cahn J.W. and Hilliard J.E., *Nucleation in a Two-Component Incompressible Fluid,* J. Chem. Phys. 31, p. 688, 1959

Cameron D.J. and Duncan R.G., *On the Existence of a Memory Effect in Hydride Precipitation in Cold-Worked Zr-2.5% Nb,* J. Nuclear Materials 68, p. 340, 1977

Carpenter G.J.C., *The Dilatational Misfit of Zirconium Hydride Precipitated in Zr*, J. Nuclear Materials 48, p. 264, 1973.

Carpenter G., Watters J. and Gilbert R., *Dislocations Generated by Zirconium Hydrides in Zirconium and Some of its Alloys*, J. Nuclear Materials 48, p. 267, 1973.

Christian J.W., *The Theory of Transformations in Metals and Alloys*, Pergamon Press, Oxford, p. 416, 1965

Chu H., Wu S. and Kuo R., *Hydride Reorientation in Zircaloy-4 Cladding*, J. Nuclear Materials 373, p. 319, 2008.

Chung H.M., *Understanding hydride- and hydrogen-related processes in high-burnup cladding in spent-fuel-storage and accident situations* in: *Proceedings of the 2004 International Meeting on LWR Fuel Performance*, Orlando, Florida, September 19-22, 2004

Cinbiz M.N., Motta A.T. and Koss D.A., *Hydride Reorientation in Zircaloy-4 under Different States of Stress as Studied with in-situ X-Ray Diffraction,* J. Nuclear Materials 477, p. 157, 2016

Copyright © Advanced Nuclear Technology International Europe AB, ANT International, 2018.

Colas K. B. et al., *In situ Study of Hydride Precipitation Kinetics and Re-orientation in Zircaloy using Synchrotron Radiation*, Acta Mater. 58, p. 6575, 2010.

Colas K. et al., *In-situ Study of Hydride Reorientation Kinetics using Synchrotron Radiation*, 16th ASTM Zr Symposium, Chengdu, China, 2011.

Colas K.B., *Fundamental Experiments on Hydride Reorientation in Zircaloy* , PhD. Dissertation, Pennsylvania State University, University Park, 2012

Colas K., Motta A., Daymond M.R., Almer J., *Mechanisms of Hydride Reorientation in Zircaloy-4 Studied in Situ*, in: *Zirconium in the Nuclear Industry: 17th International Symposium*, Comstock A.J., Barbéris P. (Eds.), ASTM International, West Conshohocken, PA, 10428-2959, U.S.A., STP 1543, 2014

Colas, private communication, 2017.

Coleman C. E. and Inozemtsev V. V., *Measurement of Rates of Delayed Hydride Cracking (DHC) in Zr-2.5 Nb Alloys – an IAEA Coordinated Research Project*, J. ASTM International 5, 2008, Paper ID JAI101091. (Based on IAEA Report, IAEA-TECDOC-1410, 2004), 2008.

Coleman C.E. et al., *Delayed Hydride Cracking in Zircaloy Fuel Cladding – An IAEA Coordinated Research Programme,* Nuclear Eng. & Technol. 41, p. 1, 2009

Daum R., Majumdar S., Liu Y., Billone M., *Radial-Hydride Embrittlement of High-Burnup Zircaloy-4 Fuel Cladding*, Journal of Nuclear Science and Technology 43, No.9, p.1, 2006.

Daum R., Chu Y. and Motta A., *Identification and Quantification of Hydride Phases in Zircaloy-4 Cladding Using Synchrotron X-Ray Diffraction*, J. Nuclear Materials 392, p.453, 2009.

Delobelle P., Robinet P., Geyer P., Bouiffioux P., *A Model to Describe the Anisotropic Behaviour of Zircaloy--4 Tubes*, J. Nuclear Materials 238, p. 135, 1996.

Desquines J. et al., *Influence of Temperature and Hydrogen Content on Stress-induced Radial Hydride Precipitation in Zircaloy-4 Cladding*, J. Nuclear Materials 453, p. 131, 2014.

Dutton R. and Puls M.P., *A Theoretical Model for Hydrogen Induced Sub-Critical Crack Growth*, in: *Effect of Hydrogen on Behaviour of Materials*, A.W. Thompson and I.M. Bernstein, Eds., Metal Society, 516-528, AIME, New York, 1976.

Dutton R., Nuttall K., Puls M.P., Simpson L.A., *Mechanisms of Hydrogen Induced Delayed Cracking in Hydride Forming Materials,* Metall. Trans. A 8A, p. 1553, 1977

Ells C.E., *Hydride Precipitates in Zirconium Alloys*, J. Nuclear Materials 28, p. 129, 1968.

Ells C.E., *The Stress Orientation of Hydride in Zirconium Alloys*, J. Nuclear Materials 35, p. 306, 1970.

Eshelby J.D, *The Continuum Theory of Lattice Defects*, in: *Solid States Physics*, Seitz F., Turnbull D.(Eds.), Vol. 3, p. 79, Academic Press, New York, 1956

Eshelby J.D. *The Determination of the Elastic Field of an Ellipsoidal Inclusion, and Related Problems,* Proc. Roy. Soc. A241, p. 376, 1957

Eshelby J.D., *Elastic Inclusions and Inhomogeneities,* in: *Progress in Solid Mechanics*, Snedden N. I. and Hill R., Eds., Vol. 2, p. 89, North Holland, 1961

Fielding L.C.D., *The Bainite Controversy,* J. Mater. Sci. & Techno. 29, p. 383, 2013

Flanagan T.P., Park C.-N. and Oates W.A., *Hysteresis in Solid State Reactions,* Prog. Solid St. Chem. 23, p. 291, 1995

Flanagan M.E., in: *Proc. 2008 Water React. Fuel Perf. Meeting,* Seoul, Korea, 2008

*Copyright © Advanced Nuclear Technology International Europe AB, ANT International, 2018.*

# Acronyms and Abbreviations

| | |
|---|---|
| DHC | Delayed Hydride Cracking |
| TSS | Terminal Solid Solubility |
| TSSD | Terminal Solid Solubility Dissolution |
| TSSP | Terminal Solid Solubility Precipitation |
| TSSP1 | Terminal Solid Solubility Precipitation 1 |
| TSSP2 | Terminal Solid Solubility Precipitation 2 |
| SAR | Stand Alone Report |
| PFM | Phase Field Methodology |
| ID | Inner Diameter |
| OD | Outer Diameter |
| SEM | Scanning Electron Microscope |
| TEM | Transmission Electron Microscope |
| XRD | X-Ray Diffraction |
| RXA | Recrystalized Annealed |
| RD | Rolling Direction of a plate |
| WD | Width Direction of a plate |
| TD | Transverse Direction of a plate |
| ND | Normal Direction of a plate |
| SRA | Stress Relieved Annealed |
| wppm | weight parts per million |
| hcp (h.c.p.) | hexagonal close packed |
| fcc | face centred cubic |
| EBSD | Electron Back Scattering Diffraction |
| PHWR | Pressurized Heavy Water Reactor |
| PWR | Pressured Water Reactor |
| RHT | Radial hydride precipitation Heat Treatment (also Radial Hydride Treatment) |
| HRT | Hydride Reorientation Treatment |
| CCT | C-shaped Compression Test |
| ASTM | American Society of Testing and Materials |
| CWSR | Cold Worked Stress Relieved |
| FE | Finite Element |
| 2-D, 3-D | Two (2) or three (3) Dimension |
| RHF | Radial Hydride Fraction |
| F-ANP | Framatom Advance Nuclear Products |
| HBR | H.B. Robinson (reactor) |
| CTDT | Cladding Tube Deformation Test |
| RT | Room Temperature |
| BWR | Boiling Water Reactor |
| DSC | Differential Scanning Calorimeter |
| DEM | Dynamic Elastic Modulus |
| FWHM | Full Width Half Maximum |
| HAZ | Heat Affected Zone |
| ODF | Orientation Distribution Function |
| HT | Heat Treatment |
| PLTS | Pure Lattice Transformation Strain |
| PLST | Pure Lattice Strain Transformation (same meaning as PLTS) |
| IPST | Invariant Plane Strain Transformation |
| PSTS | Pure Shear Transformation Strain (same meaning as IPST) |
| CANDU™ | CANada Deuterium Uranium |
| CCD | Charge Coupled Device |
| KS | Khachaturyan Shatalov |
| IF | Internal Friction |

Copyright © Advanced Nuclear Technology International Europe AB, ANT International, 2018.

# Nomenclature

Nomenclature used by this author:

| | |
|---|---|
| $J^*$ | time-dependent nucleation rate (the superscript $^*$ denotes quantities evaluated at the size of the critical nucleus) |
| $Z$ | Zeldovich non-equilibrium factor |
| $\beta^*$ | rate at which atoms are added onto the critical nucleus |
| $N$ | number of atomic nucleation sites per unit volume |
| $r_H$ | atom ratio H/Zr |
| $\beta_{phas}$ | number of energetically equivalent interstitial H sites per Zr atoms in a phase, with $\beta_{phas} = 1, 1, 1.5, 2$ for $phas =$ α–Zr, γ–, δ– and ε–hydride phases, respectively |
| $c_H$ | $= r_H/\beta_{phas}$ |
| $c_H^\beta$ | H/Zr mole (or atom) ratio of solute component (H in this text) in the critical nucleus (where β designates the precipitate phase, which for hydrides could be either the δ, γ or ε phase) |
| $\Delta G^*$ | Gibbs free energy of activation for critical nucleus formation |
| $\tau$ | nucleation incubation time |
| $t$ | isothermal reaction (hold) time |
| $k_B T$ | product of Boltzmann constant and absolute temperature, respectively |
| $n$ | number of atoms in an embryo |
| $n^*$ | number of atoms in the critical nucleus |
| $\Delta G^o$ | Gibbs free energy change for the formation of a cluster of $n$ solute atoms |
| $S^*$ | disordered area of the critical nucleus (i.e., the area of the nucleus over which single solute atoms could be added) |
| $D$ | appropriate diffusivity |
| $c_H^\alpha$ | atom fraction of solute (H) in the α–Zr matrix phase ($\equiv r_H/\beta_{\alpha\text{–Zr}} = r_H$) since $\beta_{\alpha\text{–Zr}} = 1$ |
| $a^*$ | major axis of critical nucleus when modelled as having the shape of an oblate spheroid, or radius when modelled as a disc |
| $c_H^o$ | H/Zr atom ratio of solute (H) in the supersaturated solution of the α–Zr phase; this is equivalent to $c_H^\alpha$, but denoted here by $c_H^o$ to indicate that in a closed system – cooling from a temperature at which all hydrides had been dissolved – it is the total hydrogen content in the solid |
| $D_H^v$ | volume diffusion coefficient of the solute (H) |
| $d$ | jump distance of solute (H) in the matrix (α–Zr) phase (≈ one lattice parameter) |
| $\boldsymbol{\sigma}$ | applied and/or residual stress vector |

Copyright © Advanced Nuclear Technology International Europe AB, ANT International, 2018.

# Unit conversion

| TEMPERATURE | | |
|---|---|---|
| °C + 273.15 = K | °C × 1.8 + 32 = °F | |
| T(K) | T(°C) | T(°F) |
| 273 | **0** | 32 |
| 289 | 16 | 61 |
| 298 | 25 | 77 |
| 373 | **100** | 212 |
| 473 | **200** | 392 |
| 573 | **300** | 572 |
| 633 | 360 | 680 |
| 673 | **400** | 752 |
| 773 | **500** | 932 |
| 783 | 510 | 950 |
| 793 | 520 | 968 |
| 823 | 550 | 1022 |
| 833 | 560 | 1040 |
| 873 | **600** | 1112 |
| 878 | 605 | 1121 |
| 893 | 620 | 1148 |
| 923 | 650 | 1202 |
| 973 | **700** | 1292 |
| 1023 | 750 | 1382 |
| 1053 | 780 | 1436 |
| 1073 | **800** | 1472 |
| 1136 | 863 | 1585 |
| 1143 | 870 | 1598 |
| 1173 | **900** | 1652 |
| 1273 | **1000** | 1832 |
| 1343 | 1070 | 1958 |
| 1478 | 1204 | **2200** |

| Radioactivity | |
|---|---|
| **1 Sv** | = 100 Rem |
| **1 Ci** | = $3.7 \times 10^{10}$ Bq = 37 GBq |
| **1 Bq** | = 1 $s^{-1}$ |

| MASS | |
|---|---|
| kg | lbs |
| 0.454 | **1** |
| **1** | 2.20 |

| DISTANCE | |
|---|---|
| x (µm) | x (mils) |
| 0.6 | 0.02 |
| **1** | 0.04 |
| 5 | 0.20 |
| **10** | 0.39 |
| 20 | 0.79 |
| 25 | 0.98 |
| 25.4 | **1.00** |
| **100** | 3.94 |

| PRESSURE | | |
|---|---|---|
| bar | MPa | psi |
| **1** | 0.1 | 14 |
| 10 | **1** | 142 |
| 70 | 7 | 995 |
| 70.4 | 7.04 | **1000** |
| **100** | 10 | 1421 |
| 130 | 13 | 1847 |
| 155 | 15.5 | 2203 |
| 704 | 70.4 | **10000** |
| **1000** | 100 | 14211 |

| STRESS INTENSITY FACTOR | |
|---|---|
| MPa√m | ksi√inch |
| 0.91 | **1** |
| **1** | 1.10 |

*Copyright © Advanced Nuclear Technology International Europe AB, ANT International, 2018.*